Concurrent Design Optimization of Tether-Net System and Actions for Reliable Space-Debris Capture

Chen Zeng*, Grant R. Hecht†, Souma Chowdhury‡, and Eleonora M. Botta§
University at Buffalo, Buffalo, NY, 14226

Tether-nets deployed from a chaser spacecraft are a promising solution to capturing space debris. The success of the one-shot capture process depends on the net's structural dynamic properties, attributed to its physical design, and on the ability to perform an optimal launch and closure subject to sensing and actuation uncertainties. Hence, this paper presents a reliability-based optimization framework to simultaneously optimize the net design and its launch and closing actions to minimize the system mass (Case 1) or closing time (Case 2), while preserving a specified probability of capture success. Success is assessed in terms of a capture quality index and number of locked node pairs. Gaussian noise is used to model the uncertainties in the dynamics, state estimation, and actuation of the tether-net, which is propagated via Monte Carlo sampling. To account for uncertainties and ensure computational efficiency, given the cost of simulating the tether-net dynamics, Bayesian optimization is used to solve this problem. Optimization results show that mission success rate in the presence of uncertainties is increased from 75% to over 98%, while the capture completion time is almost halved.

Nomenclature

C_m = constrained mass of tether-net system

C_p = constrained probability of successful capture

D_{rnd} = distance to target uncertainty

d_c = net closing displacement

d_L = net distance to target

d_{rnd} = closing displacement uncertainty

I_{CQ} = capture quality index

A preliminary version of this work was presented as AIAA Paper 2021-3103 at AIAA AVIATION 2021 Forum, Virtual Event, August 2-6, 2021

*Ph.D., Department of Mechanical and Aerospace Engineering, AIAA member.

†Ph.D., Department of Mechanical and Aerospace Engineering, AIAA member.

‡Associate Professor, Department of Mechanical and Aerospace Engineering, AIAA Associate Fellow.

§Assistant Professor, Department of Mechanical and Aerospace Engineering, AIAA senior member. Corresponding author. Email: ebotta@buffalo.edu

I^*_{CQ} = settled capture quality index

L_c = reference distance

L_n = net side length

m_a = estimated total net mass

m_c = mass of a corner mass

$\mathcal{N}$ = normal distribution

N_{MC} = number of Monte Carlo samples

n_L = locked node-pair count

P^*_s = observed probability of successful capture

q_n = distance between the centers of mass of the net and target

r_n = net thread radius

S_n = surface area of convex hull approximation of net

S_t = surface area of target

T = time of capture

U = uniform distribution

$\mathbf{V}_e$ = corner mass launch velocity

V_n = volume of convex hull approximation of net

V_t = volume of target

$\mathbf{X}$ = vector of decision variables

α_{rnd} = target orientation uncertainty

θ^i_{rnd} = corner mass launching polar angle uncertainty

ν^i_{rnd} = corner mass launching speed uncertainty

ρ = density

ϕ^i_{rnd} = corner mass launching azimuth angle uncertainty

I. Introduction

Tether-nets deployed from spacecraft are gaining attention as a method to remove large pieces of space debris from Earth orbit. Studies have demonstrated that Active Debris Removal (ADR) missions should be directed to the disposal of the largest and most massive pieces of debris on orbits with the highest probabilities of collisions, as they represent the highest risk for collisions which could lead to a cascaded increase in the number of space debris in orbit [1, 2]. Tether-nets are especially well-suited to the capture of large, not perfectly known objects.

A tether-net system is designed such that it consists of a tether, a net, and a set of corner masses. The net is typically

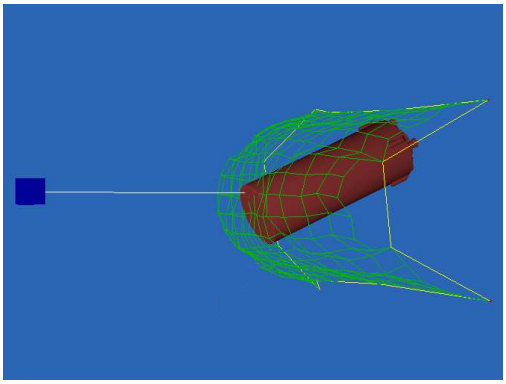

Fig. 1 Illustration of Net-Based Capture

designed to be square with four corner masses attached to the corners of the net by means of threads. Both the net and corner masses are ejected from a chaser spacecraft within close proximity of the target. The net is deployed by the tension initiated by the shooting of the corner masses, then envelops the debris and is closed around it by means of a dedicated closing mechanism. Once the target is captured, the tether provides a link between the chaser spacecraft and target such that the latter may be pulled to a disposal orbit (see Figure 1 for an illustration). When compared to conventional robotic arms, tether-net systems provide a number of benefits. They are well suited to capture large, non-cooperative pieces of space debris, often characterized by uncertain geometrical and inertial properties, and devoid of dedicated attachment features. Moreover they are less massive than robotic arms, and allow performing the capture from a larger distance from the target debris, thereby reducing the risk of dangerous collisions in ADR missions [3, 4]. Finally, net-based capture results in distributed loading on the captured object, thereby reducing the risk of generating more pieces of debris [5].

Several simulations of tether-net systems for ADR have been performed recently [6–11]. For characterization of the net deployment process, some authors have proposed performance criteria and have analyzed, by means of simulations, the effects of the geometry, mass properties, and launch conditions of the net on its dynamics [6, 7, 9, 10, 12–14]. Botta et al. also performed analysis on energy and momentum distribution to identify key parameters impacting the deployment dynamics [12]. However, a majority of the existing works have assumed the net system to be designed for the successful capture of a specific target with ideal, symmetric net launch conditions, centered with respect to the target.

Multiple authors have also studied the capture process of tether-net systems for ADR, including Salvi [9], Benvenuto et al. [15], Botta et al. [11, 16], Shan et al. [17], and more recently Si et al. [18], Huang et al. [19], Hou et al. [20], and Endo et al. [21, 22]. However, only a few works studied the capture of space debris under non-ideal conditions. Salvi examined the failure of corner mass ejection on the target capture [9]. Botta et al. [16] classified net capture missions – without a closing mechanism – as successful or failed based on scenarios where the target position and orientation varied from a nominal case, and in presence of net ejection failures. Chen et al. [23] studied the robustness

of a tether-net system equipped with a closing mechanism subject to random Gaussian noise in the target pose and net launch parameters, and showed that the system is capable of performing capture in the presence of errors with magnitude expected in real missions. Endo et al. studied the success of capture with the variation of initial net-target distance, net launch conditions, and target size [21]. To date, the only on-orbit demonstration mission of net-based debris removal was reported by Forshaw et al. [24] and Aglietti et al. [25], which comprises the complete process of planning, designing, and executing a capture mission, albeit in the absence of a tether; however, this work was focused solely on a single known (mock) target with a defined mission scenario in mind, as opposed to exploring systematic approaches that could generalize to a wide range of targets and capture conditions.

A key challenge to developing a systematic generalized framework for modeling and designing tether-net-based debris capture systems is the lack of target-agnostic metrics to evaluate the success of capture. Previous seminal work by Ravichandra and Botta [26] and Barnes and Botta [27] proposed a *Capture Quality Index (CQI)*, to measure in a quantitative way, without the need for visual inspection, the quality of the capture of a target with a net. More recently, an alternative index has been proposed by Endo et al. [22]. However, none of these measures themselves provide information on the control effort and time efficiency of the capture process.

The key to effective and economical operation of a tether-net system for space debris removal is the robustness of the system in the presence of sensing and actuation uncertainties, and the overall safety of the process [10]. This is especially critical since deployment of the tether-net is likely to be a one-shot process, i.e., the same net cannot be deployed more than once. In operations, uncertainties can be attributed primarily to inaccuracies in the control of net launch and to the imperfect state estimation of the debris. There is a critical need to identify systematic computational methods to determine system parameters that allow controlling the net deployment and capture in a manner that satisfies operational constraints under uncertainties.

Operational constraints that ensure successful capture call for the formulation of metrics that quantify the capture quality, which can then be used to systematically optimize the design and control of the tether net system. In previous work, Shah et al. investigated the optimization of launching and closing actions only to maximize the probability of successful capture under uncertainties, and found that, despite the presence of noises, the optimized launching velocities and closing displacement exhibited a probability of successful capture of up to 99% [28]. Motivated by the ease of achieving a high probability of successful capture when optimizing the actions alone under uncertainty in prior work, the present work proposes a methodology to optimize both the net design and actions concurrently while constraining the probability of successful capture and attempting to minimize performance metrics. This paper first proposes quantitative performance metrics that track operational robustness through the stages of launching and closing the net. Secondly, these metrics are used to develop a computational design automation framework that can be used to optimize the design of the net and its launch and closing parameters with the objective of maximizing the success of capture under uncertainties.

The overall problem formulation aims to explore variations in the net design (in terms of net size and mass of the corner masses), and in the net launch and capture parameters, which can jointly optimize a given objective, subject to probabilistic constraints that ensure the desired level of capture success under uncertainties. In this problem, uncertainties are associated with inadequate modeling of the system's dynamics, imperfect sensing and state estimation, and imperfect actuation mechanisms underlying net launch and closure. These can be modeled simply as added noise to the state and action parameters that are affected by the stated uncertainties. The two different objectives considered here include the mass of the tether-net system and the overall time taken from launch till the end of the closing action.

The primary contributions of this paper are thus as follows: 1) The formulation of a capture quality index and the quantification of the probability of successful target capture under uncertainties. 2) The construction of an end-to-end simulation-based optimization framework to optimize the net's physical design and launching/closing actions with tractable computational efficiency. 3) Demonstration of how design outcomes differ when the system mass is minimized, and when the mission completion time is minimized, as well as the exploration of the extent to which these designs are affected by the level of uncertainty (modeled as noise in state and action parameters) compared to a baseline design.

This is achieved by means of a surrogate-based design optimization under uncertainty approach. Specifically, Bayesian Optimization [29, 30] is employed with a multi-body capture simulation environment that serves as the high-fidelity evaluation of the net motion and target capture. The mission scenario of interest features a debris target at a known distance from the chaser spacecraft, with no relative linear and rotational velocities. Separate case studies are conducted to investigate the performance of the tether-net when the closure process is optimized alone and when the launch and closure processes are optimized concurrently.

The remainder of this paper is organized as follows: A description of the tether-net system and of the computational models implemented in simulation to analyze the motion of the launched net and its contact with the target debris are presented in Section II. The design parameters, key quantities of interest, and optimization formulations are described in Section III. Section IV presents the computational implementation of the optimization framework, and Section V discusses the optimization results, demonstrating the robustness of the optimal launching and wrapping behaviors. Finally, concluding remarks, along with ideas for future work, are summarized in Section VI.

II. Modeling of Net-Based Debris Capture

A. Target-Specific Mission Scenario

In the net-based ADR concept, the tether-net system is initially stowed in a small chaser spacecraft that approaches its debris target through a series of maneuvers, until the distance from the target is between 10−50 m. Following previous work [11], a target-specific mission scenario is defined here with the following assumptions: The geometry of the debris target is modeled after the second stage of a Zenit II rocket. The target is considered to have negligible

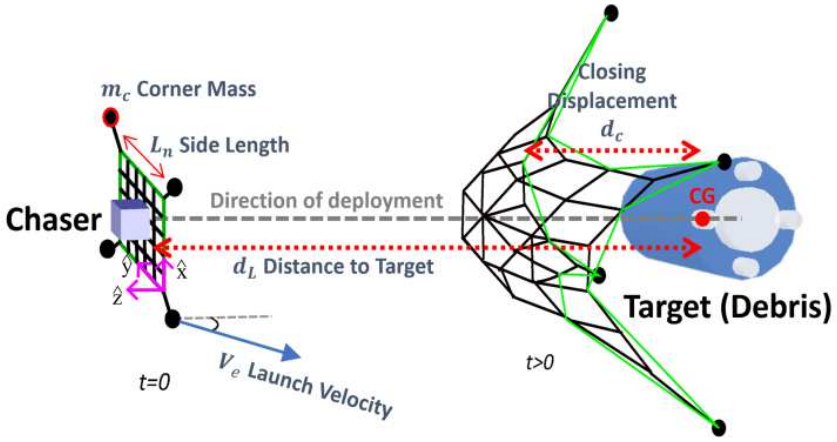

Fig. 2 Sketch of the Simulated System Dynamics and Definition of Design Space Variables

translational motion with respect to the chaser vehicle, and negligible rotational motion. The chaser vehicle is perfectly aligned with and aimed toward the center of the target, although the orientation of the target can be random. The physical configurations of the tether-net (e.g., its geometry and material), along with baseline launching conditions, are extracted from a parallel study on reliability-based co-design of the tether-net. [28]

B. Tether-Net System Configuration

The tether-net system consists of a square net with four corner masses attached to the corners of the net through corner threads, as shown in Figure 2. The net is connected to the chaser spacecraft by means of a tether with one end attached to the node at the center of the net and the other extremity reeled on a winch placed on a side of the chaser. The net is pulled out of a canister on the chaser by four corner masses, which are ejected toward the debris by a dedicated mechanism. As the net approaches the debris, a closing mechanism is activated to close the net mouth around the target, which ensures the debris remains contained in the net when the chaser pulls it to a disposal orbit.

The closing mechanism used in this work is a winched drawstring threaded along the net perimeter (shown as the green thread in Figure 2). The closing thread is winched independently from the main tether [11] and passes through 12 nodes on the perimeter, including the four corner masses. The 12 nodes are selected such that they divide each side of the net into three equal parts, similarly to what was done in previous work [11].

C. Modeling of the Tether Net and its Design Variable Space

The net is modeled with the standard lumped-parameter approach. In the Vortex-Studio-based implementation of this model (see [11]), the mass of the net is lumped into small spherical rigid bodies placed at the physical knots of the net and referred to as *nodes*. The axial stiffness and damping properties of the net's threads are represented with massless springs and dampers in parallel between the nodes. The chaser spacecraft is modeled as a cubic, free-floating rigid body. The main tether, linking the net to the chaser, is represented with a series of slender rigid bodies; relaxed

Table 1 Configurable Variables with Corresponding Boundaries

Type	Property	Lower Bound	Upper Bound
Net Design	m_c	1.0 kg	4.0 kg
	L_n	13 m	22 m
	r_n	0.001 m	0.010 m
Launch	$\mathbf{V}_e$	$[1.0\ 1.0\ 2.0]^T$ m/s	$[6.0\ 6.0\ 10.0]^T$ m/s
	d_L	15 m	35 m
Closure	d_c	-2.5 m	2.5 m

prismatic joints are used to simulate its axial and bending stiffness, as well as its damping properties. The debris is modelled as a rigid body, with patched primitives as collision geometry.

The effect of the closing mechanism on the perimeter of the net is modeled via forces and distance joints. When the closing mechanism is activated in the simulation, constant forces are made to act between each pair of adjacent nodes along the closing mechanism, which brings the nodes together. When the nodes along the closing mechanism are close enough to each other, distance joints are enabled to lock the mechanism and hold the adjacent nodes together for the rest of the maneuver. For further details of how the net motion and closing are modeled, the interested reader is advised to consult previous work [11].

In order to study and maximize the performance of the tether-net system for debris capture, three physical design parameters and three control parameters are considered, which are varied and optimized. As listed in Table 1, the design parameters include the mass of each of the corner masses (all assumed to be equal), the side length of the net, and the thickness of the threads of the net. Each of these parameters affects the motion of the net through its deployment, as well as its coverage of and contact with the debris in capture. The control parameters include the launch velocity of one of the corner masses (the other three corner masses having velocities with components of the same magnitude and signs such that deployment is symmetric), the distance from the launching point to the target prior to the launch of the net (called *distance to target*), and the z-coordinate of the relative position of the center of mass of the target with respect to the center of mass of the net at which the closing mechanism is activated (called *closing displacement*). Note that the closing displacement is a signed distance quantity, and a negative closing displacement indicates that the closing mechanism is activated while the center of mass of the net is between the chaser and the target. As given in Table 1, lower and upper bounds of the variable parameters are defined such that a wide range of designs may be explored while accounting for the geometry of the target to be captured*.

III. Design under Uncertainty Problem Formulation

*The launch velocity lower and upper bounds correspond to the absolute value of the vector components.

A. Modeling Uncertainties in the Simulated Mission and Probability of Capture Success

The majority of uncertainties in the tether-net system are due to imperfections in sensors, actuators, or computational models that inform estimation and control, which can be collectively called *systemic* uncertainties. The non-deterministic dynamics of the flexible multi-body net system are seen as *aleatoric* uncertainty, as the movement of the net during launch and wrapping can vary even under practically similar conditions. Significant systemic uncertainties include: 1) state estimation of the chaser spacecraft and of the debris target, 2) estimating the state of the launched net (or conversely modeling of the net dynamics), 3) net ejection timing and velocity, and 4) timing and speed of the net closure by means of the closing mechanism. For implementation purposes, uncertainty is directly modeled as noise added to the parameters of interest, namely to the control parameters (launch velocity and closing displacement) and the state parameters (distance to the target and orientation of the target).

The degree of uncertainty in state estimation depends on both sensor quality and the level of fidelity in modeling the dynamics. Similarly, the uncertainties associated with the launch and closing actions are contingent upon both state estimation uncertainties and actuator quality. These uncertainties are usually modeled as combinations of random distributions. In the absence of physical experiments or high-fidelity dynamics and sensing models for the tether-net system, the aforementioned uncertainties are modeled as Gaussian or Uniform distributions. Here, it should be noted that the noises in the launching velocities are defined in spherical coordinates, with the speed, polar angle, and azimuth angle defined as shown in Figure 3. In this work, all but the launching azimuth angle ϕ_{rnd} (i.e., the *direction* in which the desired launch velocity is perturbed) are modeled with Gaussian distributions. Under the assumption of perfect aiming (as described in Section II), the noises are unbiased (i.e., with zero mean). Table 2 lists the sources of uncertainties and their associated probability distributions. In the absence of a physical net-based capture system to base the modeled uncertainties, the probability distributions pertaining to the control parameters are selected to represent a system that can achieve the desired action with moderate accuracy. Additionally, the probability distribution corresponding to the target orientation was selected to exhibit a large variance to account for the possibility of large errors in computer vision-based sensing while enabling the design of a system with *inherent contingency* to such sensor failures or inconsistencies.

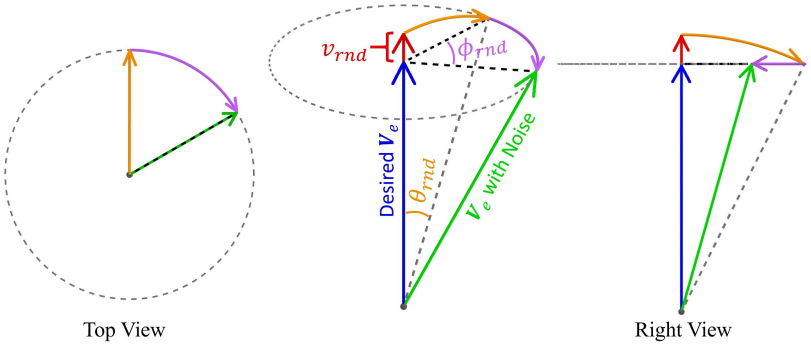

Fig. 3 Illustration of noises applied on launching velocity. Noises are applied in $v_{rnd} \rightarrow \theta_{rnd} \rightarrow \phi_{rnd}$ order.

The aleatoric uncertainty of the soft net dynamics is difficult to independently measure, let alone model. In the absence of a distribution model to describe the uncertainty of the net dynamics, direct Monte-Carlo sampling is adopted to quantify the overall impact of the uncertainties in the system. Noises (as defined in Table 2) are added to the nominal target orientation (i.e., 0°), and the desired control parameters (i.e., the target distance, launch speed and direction, and closing displacement) of a given design at the beginning of the simulations, and capture success measures are recorded at the end of the simulations.

To measure capture performance in terms of the net design and control variables, one can use the Capture Quality Index (CQI) [26, 27], which is defined as follows:

$$I_{\mathrm{CQ}} = 0.1\frac{\mid V_n - V_t \mid}{V_t} + 0.1\frac{\mid S_n - S_t \mid}{S_t} + 0.8\frac{\mid q_n \mid}{L_c} \tag{1}$$

where V_n and S_n are the volume and surface area of the convex hull approximation of the net at the n-th time step, V_t and S_t are the volume and surface area of the target, q_n is the distance between the centers of mass of the net and the target at the n-th time step, and L_c is a reference distance, i.e., the smallest distance from the center of mass of the target to its surface. Furthermore, the weights 0.1, 0.1, and 0.8 are selected specifically for the second stage of the Zenit II rocket to ensure that the CQI can distinguish between successful and unsuccessful capture, as described in [27]. Under this definition, the lower the CQI, the better the capture performance. However, as demonstrated by earlier work by the authors [28, 31]: 1) the CQI is characterized by sizable oscillations immediately after the activation of the closing mechanism (due to the rotation of the target and the motion of the net around the target), and 2) monitoring the CQI alone can lead to the possibility of false positives. Therefore, for this work, capture success is determined based on: 1) **settled CQI** (I^*_{CQ}), and 2) **locked node-pair count** (n_L). The settled CQI, I^*_{CQ}, is defined as the CQI measurement 20 seconds after the activation of the closing mechanism. The number of pairs of the closing mechanism that are locked (with 12 locked pairs being the maximum), n_L, is also measured 20 seconds after the activation of the closing mechanism and signifies that the nodes of the closing mechanism have come close together. The success thresholds of I^*_{CQ} and n_L are set as 2.0 and 10, respectively.

Based on the definition of capture success, the observed probability of success (P^*_s) is computed through the following expression:

$$P^*_s = \frac{\sum_{N_{\mathrm{MC}}}(I^*_{\mathrm{CQ}} \leq 2 \cap n_L \geq 10)}{N_{\mathrm{MC}}} \times 100\% \tag{2}$$

where N_{MC} represents the number of Monte Carlo (MC) samples. To avoid overestimating the success rate, the conditions of Eq. (2) are slightly biased towards false negatives (i.e., such that a successful capture could fail to meet I^*_{CQ} and n_L thresholds, but not vice versa).

Table 2 Modeled Uncertainties in Simulation

Noise Source	Data Type	Distribution	Units
Distance to Target (D_{rnd})	Scalar	$\mathcal{N}(0, 0.25)$	m
Target Orientation (α_{rnd})	Scalar (angular)	$\mathcal{N}(0, 45)$	deg
Launching Speed ($v_{\text{rnd}}^{(1,\dots,4)}$)*	Scalar	$\mathcal{N}(0, 0.25)$	m/s
Launching Polar Angle ($\theta_{\text{rnd}}^{(1,\dots,4)}$)*	Scalar (angular)	$\mathcal{N}(0, 2)$	deg
Launching Azimuth Angle (ϕ_{rnd})*	Scalar (angular)	$U(0, 360)$	deg
Closing Displacement (d_{rnd})	Scalar	$\mathcal{N}(0, 0.1)$	m

* Noises of launching velocities are defined in spherical coordinates (see Figure 3).

B. Design Optimization Problem Formulation

Although nets have several advantages over robotics arms, such as simplicity and flexibility to the target's shape, it is unlikely that the launch could be repeated if issues arise. Therefore, when it comes to designing the tether-net system for space operation, the reliability of the system, i.e., the success rate of the mission, is a top priority. In previous work [28], it was discovered that achieving nearly 100% mission success rate in the simulated non-nominal conditions is readily feasible (possibly due to the inherited robustness of the tethered net configuration), which suggests that maximizing the reliability alone is easily achievable. However, this comes at the expense of other performance factors, such as overall system mass and closing time or closing effort. For example, the optimized design in [28] resulted in a heavy system, of 50 kg. A more strategic optimization formulation could allow using a lighter system without compromising reliability.

In this paper, the performance of the tether-net is explored in terms of three metrics: **reliability**, **total mass**, and **completion time**. The reliability metric is represented by the capture success rate under uncertainties, which is computed via the Monte Carlo sampling and set as a constraint, leading to a reliability-based optimization formulation. The average completion time is obtained through MC sampling, where in each sample the completion time is measured from the launch of the net to 20 seconds after the closing mechanism is activated; in fact, by this time, the net movement is mostly settled. The mass of the net is estimated as a function of the net design parameters (defined in Table 1), as:

$$m_a = 38 L_n \pi r_n^2 \rho + 4 m_c \tag{3}$$

The net features a 17-by-17-node grid, resulting in a total of 38 threads (including an approximation of the closing threads). A main thread connects the net to the chaser vehicle, whose mass is not considered in our case studies and thus excluded from m_a.

In the following, two different optimization case studies are introduced, which focus on minimizing the total mass and the completion time, respectively. In both cases, the capture success rate is posed as an optimization constraint that is capped at 98% due to the limited resolution of the MC sampling.

1. Case Study 1: Minimizing Tether-net System Mass

Case Study 1 minimizes the mass of the tether-net system with the constraint of success rate in the presence of uncertainties. The optimization problem formulation is defined as follows:

$$\min_{\mathbf{X}}: \quad f_1(\mathbf{X}) = m_a(\mathbf{X}) \tag{4a}$$

$$\text{s. t.} \quad \mathbf{X} \in [\mathbf{X}_L, \mathbf{X}_U] \tag{4b}$$

$$g_1 = P_s^*(\mathbf{X}, D_{\text{rnd}}, \alpha_{\text{rnd}}, \phi_{\text{rnd}}, v_{\text{rnd}}^{(i)}, \theta_{\text{rnd}}^{(i)}, d_{\text{rnd}}) \geq C_P \tag{4c}$$

$$\text{while:} \quad \mathbf{X} = [m_c, L_n, r_n, d_L, \mathbf{V}_e, d_c] \tag{4d}$$

$$D_{\text{rnd}} \in \mathcal{N}(0, 0.25) \tag{4e}$$

$$\alpha_{\text{rnd}} \in \mathcal{N}(0, 0.25\pi) \tag{4f}$$

$$v_{\text{rnd}}^{(i)} \in \mathcal{N}(0, 0.25), \ i \in [1, ..., 4] \tag{4g}$$

$$\theta_{\text{rnd}}^{(i)} \in \mathcal{N}(0, \pi/45), \ i \in [1, ..., 4] \tag{4h}$$

$$\phi_{\text{rnd}} \in U(0, 2\pi) \tag{4i}$$

$$d_{\text{rnd}} \in \mathcal{N}(0, 0.1) \tag{4j}$$

Limited by the sampling resolution of the MC set (of 100 samples), an overly restricted success rate constraint is not feasible. The constrained value of P_s^* is therefore configured as $C_p = 98\%$.

2. Case Study 2: Minimizing Completion Time

In Case Study 2, the time to complete the capture process is minimized, with constraints on the success rate and the total mass. Equation (5) describes the optimization formulation.

$$\min_{\mathbf{X}}: \quad f_2(\mathbf{X}) = \frac{\sum_{N_{\mathrm{MC}}} T_j(\mathbf{X})}{N_{\mathrm{MC}}} \tag{5a}$$

$$\text{s. t.} \quad \mathbf{X} \in [\mathbf{X}_L, \mathbf{X}_U] \tag{5b}$$

$$g_1 = P_s^*(\mathbf{X}, D_{\mathrm{rnd}}, \alpha_{\mathrm{rnd}}, \phi_{\mathrm{rnd}}, v_{\mathrm{rnd}}^{(i)}, \theta_{\mathrm{rnd}}^{(i)}, d_{\mathrm{rnd}}) \geq C_P \tag{5c}$$

$$g_2 = m_a(\mathbf{X}) \leq C_m \tag{5d}$$

$$\text{while:} \quad \mathbf{X} = [m_c, L_n, r_n, d_L, \mathbf{V}_e, d_c] \tag{5e}$$

$$D_{\mathrm{rnd}} \in \mathcal{N}(0, 0.25) \tag{5f}$$

$$\alpha_{\mathrm{rnd}} \in \mathcal{N}(0, 0.25\pi) \tag{5g}$$

$$v_{\mathrm{rnd}}^{(i)} \in \mathcal{N}(0, 0.25),\ i \in [1, ..., 4] \tag{5h}$$

$$\theta_{\mathrm{rnd}}^{(i)} \in \mathcal{N}(0, \pi/45),\ i \in [1, ..., 4] \tag{5i}$$

$$\phi_{\mathrm{rnd}} \in U(0, 2\pi) \tag{5j}$$

$$d_{\mathrm{rnd}} \in \mathcal{N}(0, 0.1) \tag{5k}$$

Here, T_j represents the completion time of the j-th sample, and C_m = 15 kg, for the optimization trials.

While completion time by itself might be less critical than the system mass – considering that the debris capture mission typically completes within a minute – analyzing such a case sheds light on potential design trade-offs with respect to a pure mass-minimization approach. More specifically, due to potential errors in sensing and actuation (that are not necessarily represented in detail, even with the added noise, at this conceptual design stage) a longer operational time could lead to a larger accumulation of errors in capture performance. However, further fine-grain analysis is required in the future to understand whether shorter mission times indeed mitigate the propagation of uncertainties in general for this system.

IV. Simulation and Optimization Framework

A. Launch, Deployment and Capture Simulation

The deployment and capture mission is simulated in the previously-developed simulation framework based on Vortex Studio, a powerful multi-body dynamics simulation platform designed for real-time simulation of complex systems and providing built-in graphical visualization, which is free for academic use. As detailed in previous work by Botta et al. [11], the net is modeled with a lumped-parameter approach, where the mass is lumped in the physical knots of the net, and the elastic and energy dissipation properties of the net are represented by modeling each thread of the net (between two physical knots) with a constraint that is defined with spring and damping coefficients. In this framework,

all bodies in the simulation – including the masses lumped at the knots of the net and the corner masses, the elements composing the main tether, as well as the target and chaser spacecraft – are represented with rigid bodies. These are constrained with joints of different types, including distance joints for the threads of the net, a winch between the chaser and the main tether, and others. Contact dynamics is represented by specifying a collision geometry for each body in the simulation, checking for collisions at each time step of the simulation, and – in the case of collisions – computing forces of contact according to a modified Kelvin-Voigt model in which sticking is not possible for normal forces, and a scaled-box friction model (i.e., an approximation of Coulomb's friction model) for friction forces.

The effect of the closing mechanism around the perimeter of the net is modeled similarly to what was done in Reference [11]. This approach includes 1) applying constant forces (of magnitude $F_c = 2m_c L_n/25$) between each pair of contiguous nodes along the closing mechanism, which brings those nodes closer to each other, and 2) enabling distance joints (with maximum distance set to zero) once the distance between two adjacent nodes along the closing mechanism becomes lower than a small threshold (of 1 meter in this work), such that those nodes are constrained to remain together for the rest of the capture. More details on the modeling of the system and on the simulation tool can be found in previous work by Botta et al. [11].

B. Design Optimization Framework

Simulation of the dynamics of the net involves the motion of hundreds of bodies with contact dynamics, and can become prohibitively expensive, especially when MC sampling is used to compute the uncertainties. Hence, direct simulation-based optimization is computationally intractable in this case. Instead, a surrogate-based optimization or a multi-fidelity optimization approach [32] is preferred to solve the problem of optimal net design and operation. Here, Bayesian Optimization (BO) [29, 30] is used, due to its favorable performance under sparse sample evaluations and noisy outputs.

As illustrated in Figure 4, the workflow of the optimization process consists of 8 components divided into two layers: the optimizer layer (right) and the function evaluation layer (left). The optimizer layer expresses the BO process. The standard BO approach trains a Gaussian Process (GP) surrogate model of the expensive high-fidelity simulations and uses it to construct an acquisition function over which an optimization search is performed to identify the next point to be sampled in the design variables space [33]. The new sample is then added to the existing sample set, the GP function is retrained, and the process repeats until convergence or a set maximum number of high-fidelity simulations have been performed. Various choices exist with regard to the choice of kernel function within the GP model and the construction of the acquisition function. Here we use the popular Matern kernel. The sampling procedure can be parallelized for some variants of BO, but is not necessary in this work since parallel computing is already implemented for the Monte Carlo process. The acquisition function governs the direction of convergence of BO, by balancing exploration and exploitation. One of the most common acquisition functions, the Expected Improvement Plus (EI+) function, is used for

this work. The termination criterion here is set to be a hard iteration limit, which is directly relatable to a bound on the maximum number of high-fidelity simulations. To implement this optimization approach, we use the `bayesopt` library from MATLAB. Details of the optimizer setup are presented in Section V.

The function evaluation layer includes 1) noise synthesis, 2) MC sampling, 3) simulation of tether-net deployment and target capture mission, and 4) success rate evaluation. The noise synthesis segment (described in Section III.A) prepares the MC sample set with various noises for batched simulations. The MC sampling and capture mission simulation segments are essentially one step of batched simulation runs in parallel, with the simulation results checked and summarized to calculate the overall success rate in the segment of success rate evaluation.

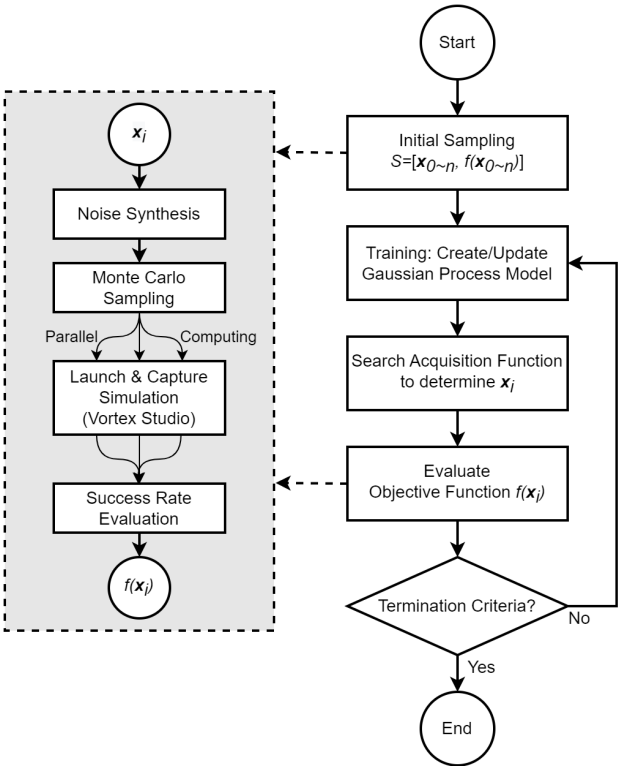

Fig. 4 Bayesian Optimization Workflow of the Tether Net Capture Mission

V. Optimization Results

In this Section, the results of baseline simulations and of the optimizations in Case Study 1 and Case Study 2 are analyzed. A design candidate based on a previous design of the tether-net system (including the net configuration, as well as the launching and closing parameters) provided by Botta et al. [11] is featured in the case studies presented in the following as one of the baselines. An additional, artificially designed baseline is also included for the sake of comparison,

A numerical experiment was conducted to determine the appropriate number of MC samples, consisting of

Table 3 Optimization Settings and Summary

CPU Model		OS	Software	
AMD 1950x (16c32t) @3.8 GHz		Windows 10	MATLAB 2020b	
Kernel Func.	Acquisition Func.	Seed Points	GP Active Set	Parallel Threads
Matern	EI+	50	200	30
Case Study	Iteration Count	Time Lapsed		
1	200	28.05 hrs		
2	200	22.67 hrs		

simulations of net launch, deployment, closure, and target capture. To ensure a reasonable trade-off between accuracy and computational cost, the MC sample set is configured as $N_{\mathrm{MC}} = 100$ for function evaluations in the optimization processes. Validation of the design candidates (which will be presented in Section V.C) is performed with a MC sample set of 1000.

The optimization trials are performed in MATLAB on a Windows 10 workstation while exploiting parallel computing on 30 threads. Table 3 lists the BO-prescribed parameters, as well as the computer configurations used for the case studies. Throughout the discussion, reference will be made to Table 4, which collects the values of the design variables of the baselines and those obtained in the optimization runs, together with the performance indices. The performance indices include the mass of the tether-net system m_a, the average capture completion time T, the estimated probability of success P_s^*, and validated probability of success (which will be defined in more detail in Section V.C).

A. The Baselines

1. Artificial Baseline Motivated by Previous Work

A baseline design was introduced by Botta et al. [11] in previous work on deployment and capture dynamics. The baseline features four 0.5 kg corner masses and threads of the net with a 1 mm radius. Actions were manually tuned to function under an ideal capture condition, without uncertainties. Benefiting from the lightweight corner masses, the total mass of the artificial baseline is of only 5.31 kg. In the artificial baseline design, the corner masses are launched at a relatively slow velocity, of 2.08 m/s, which results in a fairly long completion time (i.e., 57.2 s). When evaluated with the same level of uncertainties as in the optimization runs, the capture success rate of the baseline is of around 75%.

2. A Sub-optimal Design

In addition to the artificially designed baseline, a reliable but sub-optimal design is introduced for the purpose of comparing performances. This sub-optimal design was generated at the 17-th iteration of the Case Study 1 optimization, which is the first iteration with a success rate over 90%. The design variables and performance indices values for the

sub-optimal design are listed in the second row of Table 4. It is observed that the sub-optimal design is significantly heavier (at 29.52 kg), and that capture is achieved in less than half the time (i.e., approx. 26 s).

B. The Optimized Designs

Optimization for both case studies in Section III is performed with the iteration count limit set to 200 iterations. With the settings in Table 3, the total computing time for the optimizations in Case Study 1 and Case Study 2 is 50.7 hours overall. Optimization results are listed in the lower part of Table 4, and the convergence histories of the optimization trials are shown in Figures 5 and 6 for Case Study 1 and Case Study 2 respectively. In the following, results of the optimization cases are analyzed separately.

1. Case Study 1: Minimizing Tether-net System Mass

In Case Study 1, the mass of the tether-net system is minimized while satisfying reliability constraints, but in the absence of time constraints. Figure 5 shows the convergence history of the Case Study 1 optimization, where the grey line indicates the objective function value of the current candidate design (regardless of its feasibility, i.e., satisfaction of the constraints), while the black line indicates the best feasible design (i.e., the feasible design with the smallest objective function value) discovered thus far. Although optimization was terminated after 200 iterations, reasonable convergence is seen to occur in about 55 iterations. As shown in Table 4, the optimization result is a design that minimizes the total mass (to 7.53 kg) while satisfying the success rate constraint (98%), surpassing the reliability results from previous work [28, 31] and proving the high robustness of the tether-net design. Interesting to note is that the mass minimization is achieved by the corner masses and the thread radius both hitting their lower bounds, whereas the size of the net is near its upper limit, at 21.26 m. The launching velocity of the Case Study 1 solution is high compared to that of the artificial baseline, which results in a significant reduction in completion time even when the distance from launch to target is approximately double. Here, the closing mechanism is actuated when the center of mass of the net has traveled 2.11 meters past the target.

2. Case Study 2: Minimizing Completion Time

In Case Study 2, the time to complete the capture process is minimized, subject to reliability constraints and to the constraint that the mass of the tether-net is lower than 15 kg. Figure 6 displays the convergence history of the Case Study 2 optimization. From the top plot, we observe that the optimization process found the feasible region within the design space soon after the 23-rd iteration (when the black line – corresponding to the best feasible solution – is observed to start). The bottom two plots help confirm that this is the first time during the optimization that the values of probability of success and net mass are both below their respective constraint thresholds. Convergence in the objective, i.e., completion time, is settled for the most part after the 80-th iteration, although incremental improvements in the

Table 4 Design Variables and Performances of the Candidates

Name	m_c (kg)	L_n (m)	r_n (m)	d_L (m)	$\mathbf{V}_e$ (m/s)	d_c (m)	m_a (kg)	T (s)	P_s^*	P_s^* Validated
Artificial Baseline	0.5	20	0.001	20	$[0.40, 0.40, 2.00]^T$	0.50	5.31	57.2	-	75.2%
Sub-optimal Design	3.83	21.4	0.002	17.87	$[2.30, 4.95, 6.54]^T$	1.57	29.52	25.9	97%	96.5%
Mass Min. (Case 1)	1.00	21.26	0.001	34.15	$[2.26, 2.43, 8.55]^T$	2.11	7.53	27.4	98%	98.3%
Time Min. (Case 2)	2.05	19.84	0.001	16.14	$[4.02, 2.60, 8.88]^T$	2.26	11.89	24.2	100%	98.2%

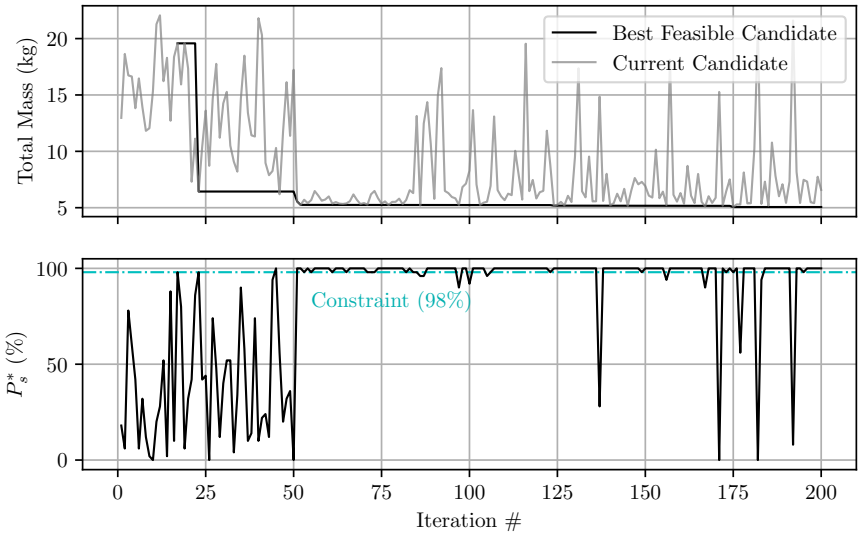

Fig. 5 Case Study 1 Convergence History

objective function were observed throughout the remainder of the trial. As seen from the results provided in the last row of Table 4, the optimal design of Case Study 2 features heavier corner masses (of approx. 2 kg) and a further delay of closing (which happens at $d_c = 2.26$ m) compared to those of the mass minimization. Notable is that – unlike the artificial baseline – the direction of launch of the corner masses in both optimizations is not symmetric with respect to the launch direction (i.e., $V_{e,x} \neq V_{e,y}$). The mission completion time is significantly shorter than that of the artificial baseline, and mildly shorter than those of the other two design candidates. This is mainly attributed to a smaller launch distance and a higher launch speed compared to that obtained in Case Study 1. The Case Study 2 optimal design is heavier (i.e., with a mass of 11.89 kg) than that of Case Study 1, but still much lighter than the sub-optimal design and lower than the set constraint. Although the reported success rate P_s^* reached 100% during the optimization trial, the validation study later showed that this estimate of perfect reliability was obtained due to inadequate statistical sampling.

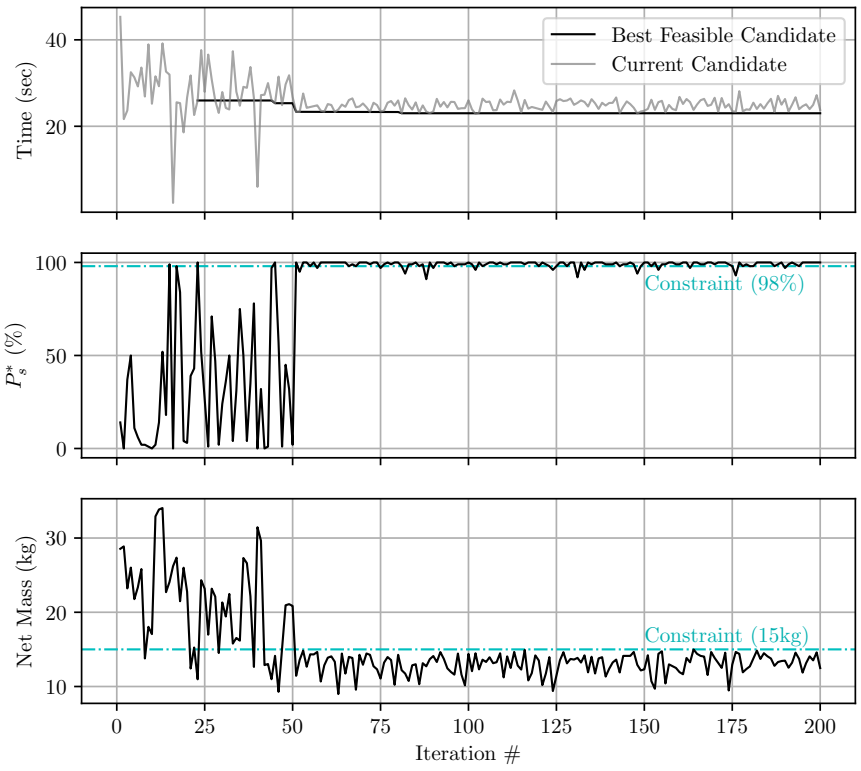

Fig. 6 Case Study 2 Convergence History

C. Validation and Verification

Validation simulations were conducted for the two optimal designs, along with the two baselines, with 1000 MC samples for each design candidate. For each MC trial, the uncertainties provided in Table 2 are modeled as described in Section III.A. The validated success rates were found to be consistent with those estimated for optimization, with errors within half a percent for the Sub-optimal Design and Case Study 1, proving the reliability of the 100-sample MC set used in optimizations. The validation simulations confirmed that the optimum designs satisfy the success rate constraint of 98%, and that the non-optimum designs do not. It is worth pointing out that the Case Study 2 (i.e., time minimized) optimum design shows only a 98.2% success rate in the validation study, down from the 100% probability of success observed in the optimization trial. The Case Study 1 (i.e., mass minimized) optimum design shows a 98.3% success rate here, which is within the margin of error of the 100-sample MC set.

Figure 7 displays CQI values over time for every MC trial (in grey) along with the mean CQI (in black) for each design candidate (baseline, sub-optimal, mass minimized and time minimized). From this plot, it can be appreciated how the variance of CQI values for both optimal designs, as well as the sub-optimal design, show a major improvement in consistency over the artificial baseline. Additionally, it can clearly be seen that the artificial baseline exhibits many trials with growing CQI values after the closing mechanism activates, indicating failed capture, which happened only once for the time-optimized design (Case Study 2) and never for the mass-optimized design (Case Study 1). This finding not only further supports the observed success rate constraint satisfaction, but also indicates that the trade-off between the total mass and mission time has been satisfactorily explored. Furthermore, rapid reduction in the CQI can be observed for the optimal design candidates, as well as the sub-optimal design, when compared to the artificial baseline, showing a clear improvement in debris capture with the application of the proposed optimization framework.

Several simulations from the validation process were also picked for visual verification through graphics rendering. Figures 8 to 11 contain snapshots of the verified simulations from each candidate, in which the system is seen 1) upon full release of the net from the chaser spacecraft, 2) at maximum opening of the net, 3) at initial wrapping of the net about the target, and 4) at successful capture. The different distances between the chaser and target, angles that the corner masses are launched at, and orientations of the target are representative of the different situations in which the target could be, and of the explored design space. As can be seen, each of the rendered simulations resulted in a successful capture. Interestingly, it can clearly be observed that the sub-optimal design exhibits the largest overall net mouth opening of the net, at $t = 4$ s, while the mass-optimal design exhibits the largest maximum opening of the net among the optimal candidates, at $t = 6$ s, shedding some light on the evolution of the Case Study 1 design through optimization. The time-optimal design displays a different behavior, with a very narrow maximum net mouth area, at $t = 2.5$ s. The last frame of each figure displays the moment the capture is settled. It is confirmed that the two optimized case studies substantially reduced the time requirement for completing the capture, from 27 seconds (for the baseline design) down to 12 seconds (for the mass minimized case) and to 7.5 seconds (for the time minimized case).

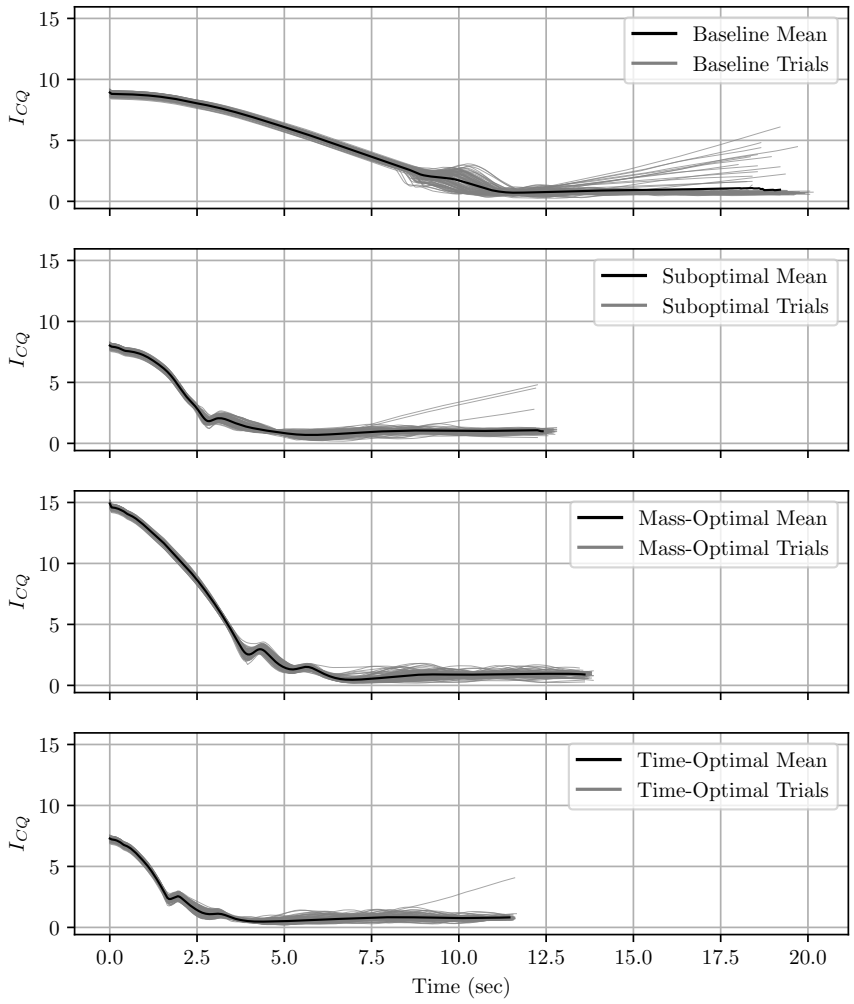

Fig. 7 Values of CQI Terms Through The Mission

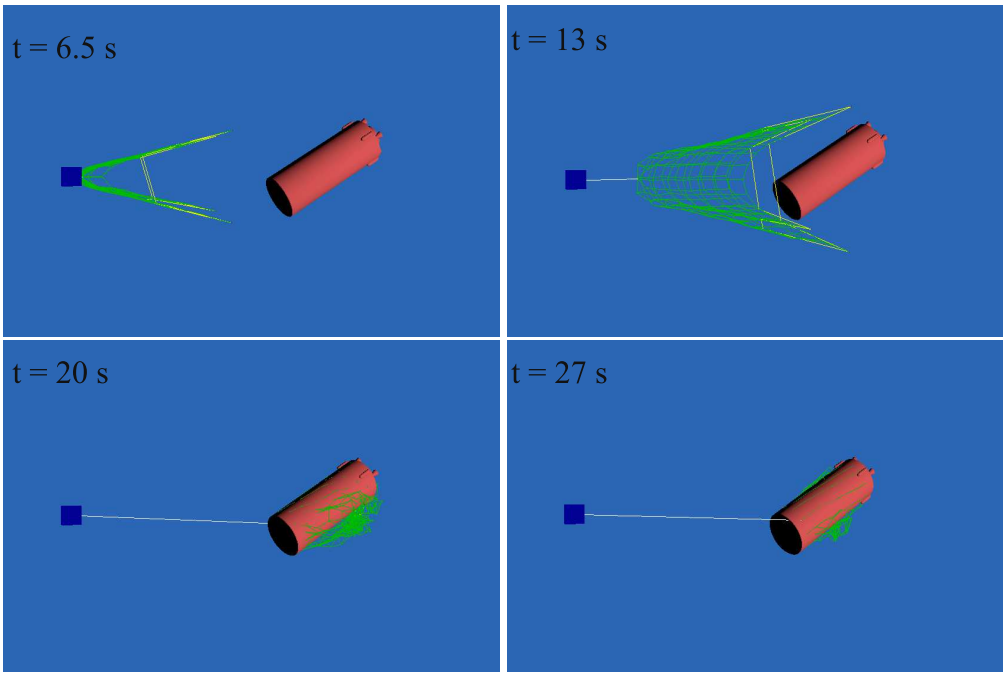

Fig. 8 Baseline Screenshots

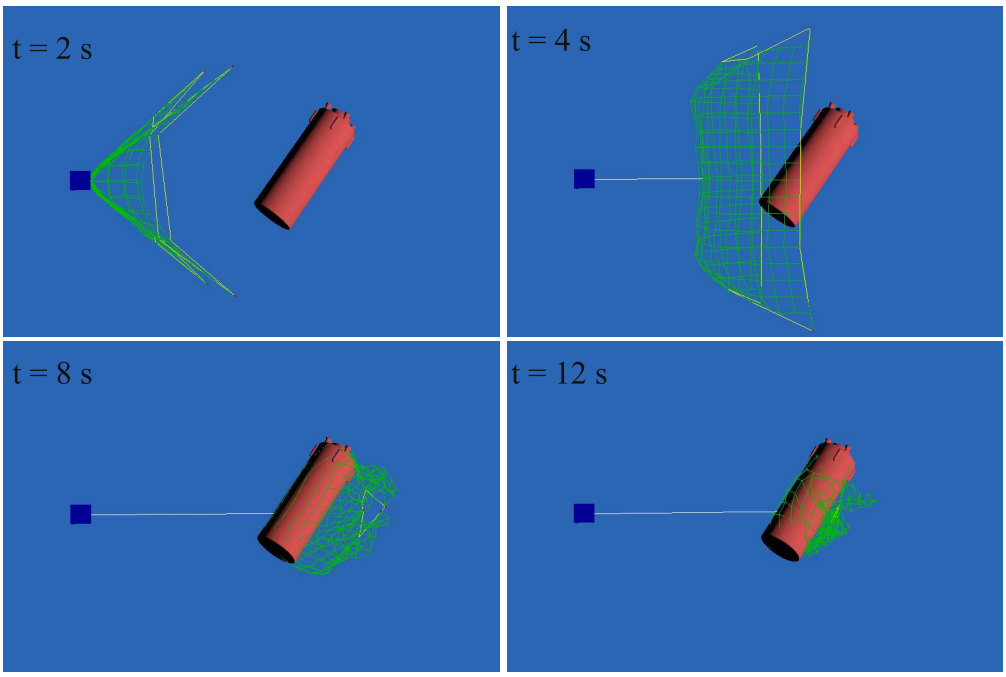

Fig. 9 Sub-Optimal Screenshots

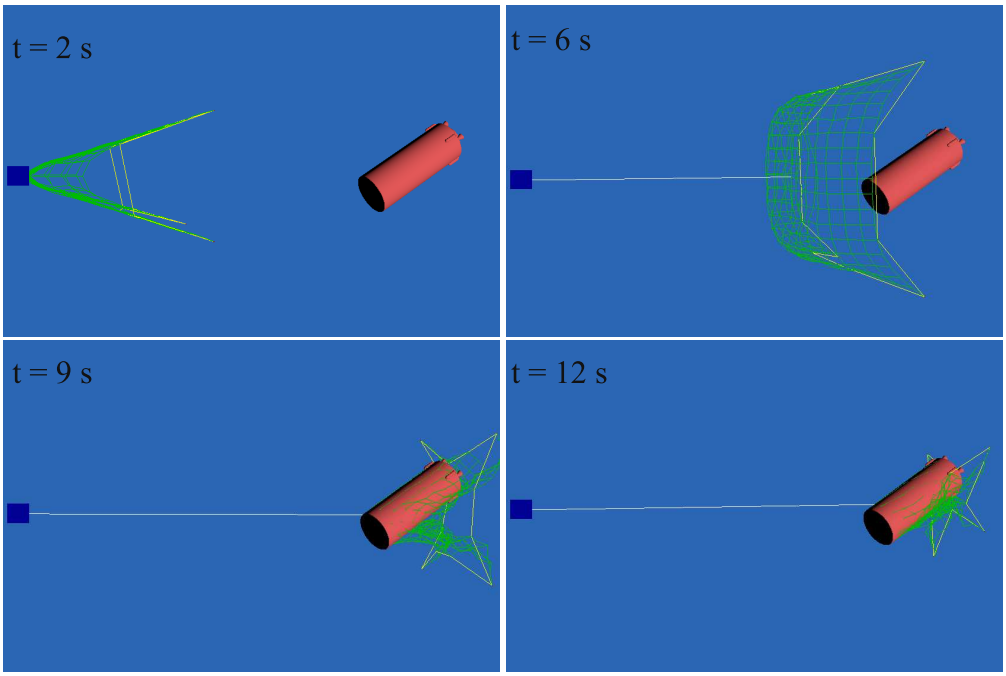

Fig. 10 Mass-Optimal Screenshots

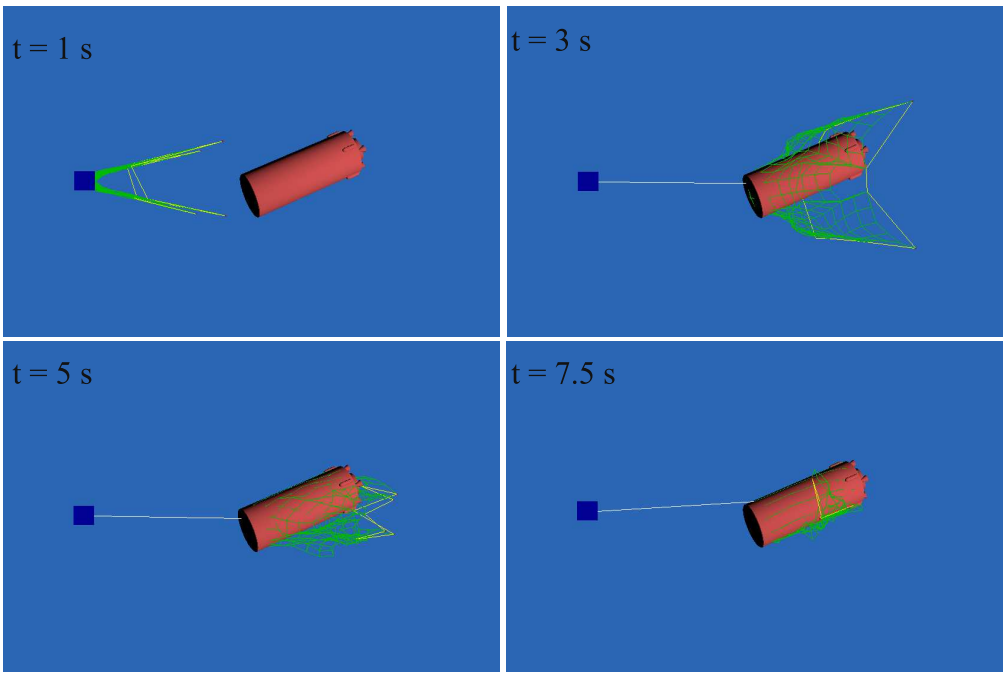

Fig. 11 Time-Optimal Screenshots

D. Noise Sensitivity Analysis

The implementation of uncertainties is in the form of zero-biased Gaussian noise in this work due to the lack of experimental data on the sources of uncertainty or error. Thus, it becomes necessary to evaluate how the optimum decisions would fare against scenarios that are drawn from different levels of uncertainty. Here, the uncertainty analysis is performed with Case Study 2 (i.e., time minimized) optimal design: the noises for the launching speed (v_{rnd}), launching polar angle (θ_{rnd}), distance to target (D_{rnd}), and closing displacement (d_{rnd}) are modified by changing the variances from 10% to 1,000% those in Table 2, and their impact on the probability of success is observed.

The probability of success corresponding to the different magnitudes of noise is shown in Figure 12. The uncertainty analysis indicates that the time-minimized optimal design is quite robust against noise in launching speed and closing displacement. This is because the success rate shows little to no degradation with up to a 10 times increase in noise. The capture success rate remains unaffected when the the noise in the launching polar angle is doubled that of the initially assumed level, but thereafter decrease to about 80% when this noise is made five fold of the original assumed value. The success rate is clearly prone to any increased noise in the distance to target, for which doubling the noise magnitude reduces the success rate by over 20%. These impacts might be attributed to the property that both the launching polar angle and the distance to target influence whether the net is opened enough upon approaching the target. The observation that the time-minimized design is not adequately robust against high noise in the launching polar angle and the distance to the target is due to the choice of a narrow launching angle in the optimal design; this choice slightly compromises robustness, albeit at the benefit of reducing the capture completion time.

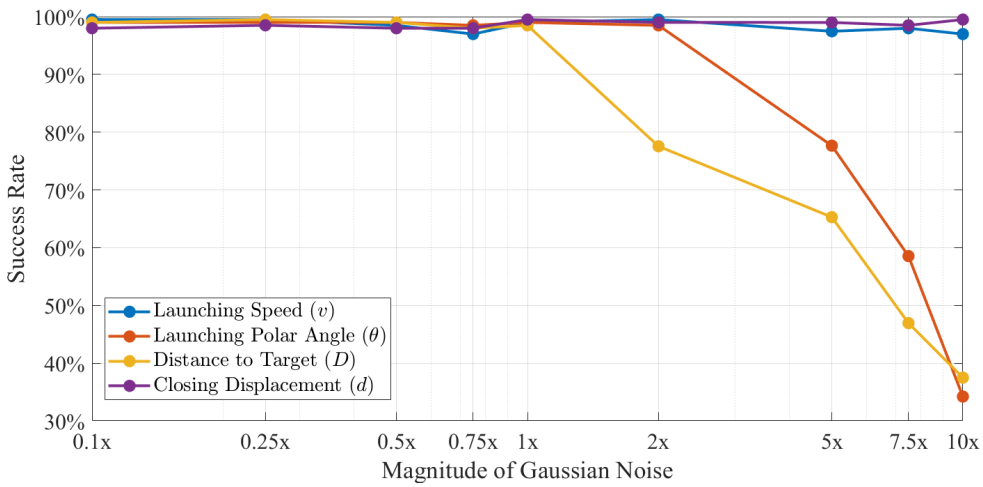

Fig. 12 Mission Success Rate for Varying Noise Levels

E. Discussion

Both of the optimal designs significantly outperform the artificial baseline in terms of capture success rate and completion time. Compared to the sub-optimal design, the optimal designs also achieve major advantages with respect to total system mass and the probability of successful capture. Moreover, both optimal designs outperform previous work [28] which solely aimed to maximize the probability of successful capture under uncertainty. This enhanced performance is evident in terms of both the overall system mass and the duration required to achieve successful capture, all while upholding a high probability of successful capture. The impact of uncertainties in driving design choices is apparent in the study, and warrants more granular future investigation with a high-fidelity resolution of the uncertainties in state and control variables, in order to design even more reliable tether-net systems. The launching speeds of both of the optimal designs were found to be significantly higher than that of the baseline, with the closing actions delayed with further offsets. The Case Study 1 optimal design minimizes the corner mass weight and the thread radius to reduce the total mass, while the Case Study 2 optimal design adopts heavier corner masses and a faster-launching velocity to speed up the motion of the net. The optimal distance from launch to target ranges from 16.14 m in Case Study 2 to 34.15 m in Case Study 1, thereby displaying marked dependence on the optimization objective. Overall, the Case Study 1 optimal design can be perceived as the optimally balanced design candidate due to its high success rate, and its low total mass, contributing to a reduction of mission costs.

We speculate from these results that the following design choices benefit the reliability of the system under uncertainty: 1) a large net geometry (with side length larger than 20 meters), 2) corner masses that outweigh the rest of the net, 3) higher launching speeds, and 4) delayed closing actions. While some of these factors might shift when control effort (or power consumption) and other cost and safety factors are taken into consideration, it is expected that the framework proposed in this work will remain applicable.

VI. Concluding Remarks

This paper introduced a simulation-to-optimization computational framework for a simple and robust tether-net-based debris capture system. A quantitative capture success evaluation was formulated based on the settled CQI and the locked node-pair count. A set of performance metrics was proposed with reliability, cost efficiency, and generalizability in mind, comprising of 1) capture success rate under uncertainty, 2) total mass of the system, and 3) mission time consumption. The computation pipeline utilizes the capture simulations based on lumped-parameter models, as well as a surrogate-based Bayesian optimizer. Uncertainties from various sources were modeled with Gaussian noises and evaluated through parallel Monte Carlo sampling.

Two case studies were performed to investigate the performance potentials of the tether-net system in terms of success rate and mass/time reduction. Through concurrent optimization of the net design and actions (i.e., launch and closure), the mission success rate was increased from 75% to over 98%, and the completion time was shortened from 57

seconds to less than 30 seconds. The optimized tether-net systems have a mass lower than 12 kg and maintain good consistency of trajectory and success despite uncertainties. Therefore, we consider the optimized tether-net system designs to be characterized by good reliability and cost efficiency. In the two case studies, Bayesian Optimization showed robustness against function stochasticity and frugality to function evaluations, which are crucial for maintaining optimality and limiting the computing cost for large-scale, nonlinear systems with uncertainties, such as the tether-net system.

In addition to showcasing the potential of the tether-net system, this work also indicates that the framework for simulation and optimization is mature for conceptual-level design. Future works will investigate additional real-world conditions, starting with a rotating target. Simulated state estimation and sensing are in the pipeline to be introduced, based on which we will study intelligent launching and wrapping control for adaptive missions.

Acknowledgments

This material is based upon work supported by the National Science Foundation under CMMI Award No.2128578. Grant Hecht also acknowledges support from the National Science Foundation Graduate Research Fellowship under Grant No. 2043091. Any opinions, findings, and conclusions or recommendations expressed in this material are those of the author(s) and do not necessarily reflect the views of the National Science Foundation.

References

[1] Kessler, D. J., "Collisional Cascading: The Limits of Population Growth in Low Earth Orbit," *Advances in Space Research*, Vol. 11, No. 12, 1991, pp. 63–66. https://doi.org/10.1016/0273-1177(91)90543-S.

[2] Liou, J.-C., "An Active Debris Removal Parametric Study for LEO Environment Remediation," *Advances in Space Research*, Vol. 47, No. 11, 2011, pp. 1865–1876. https://doi.org/10.1016/j.asr.2011.02.003.

[3] Shan, M., Guo, J., and Gill, E., "Review and Comparison of Active Space Debris Capturing and Removal Methods," *Progress in Aerospace Sciences*, Vol. 80, 2016, pp. 18–32. https://doi.org/10.1016/j.paerosci.2015.11.001.

[4] Mark, C. P., and Kamath, S., "Review of Active Space Debris Removal Methods," *Space Policy*, Vol. 47, 2019, pp. 194–206. https://doi.org/10.1016/j.spacepol.2018.12.005.

[5] "ROGER Phase-A Final Report Executive Summary," Tech. rep., Astrium Space Transportation, 2003.

[6] Chen, Q., and Yang, L., "On Dynamics of Casting a Net Structure of Flexible Cables on Orbit," *Proceedings of the 60th International Astronautical Congress*, 2009.

[7] Liu, H., Zhang, Q., Yang, L., and Zhu, Y., "Modeling and Simulation of Deployment Dynamics of Space Webs," *Proceedings of the 64th International Astronautical Congress*, 2013.

[8] Wormnes, K., De Jong, J., Krag, H., and Visentin, G., "Throw-Nets and Tethers for Robust Space Debris Capture," *Proceedings of the 64th International Astronautical Congres*, 2013.

[9] Salvi, S., "Flexible Devices for Active Space Debris Removal: The Net Simulation Tool," Master's thesis, Politecnico di Milano, 2014.

[10] Shan, M., Guo, J., and Gill, E., "Deployment Dynamics of Tethered-Net for Space Debris Removal," *Acta Astronautica*, Vol. 132, 2017, pp. 293–302. https://doi.org/10.1016/j.actaastro.2017.01.001.

[11] Botta, E. M., Sharf, I., and Misra, A. K., "Simulation of Tether-Nets for Capture of Space Debris and Small Asteroids," *Acta Astronautica*, Vol. 155, 2019, pp. 448–461. https://doi.org/10.1016/j.actaastro.2018.07.046.

[12] Botta, E. M., Sharf, I., and Misra, A. K., "Energy and Momentum Analysis of the Deployment Dynamics of Nets in Space," *Acta Astronautica*, Vol. 140, 2017, pp. 554–564. https://doi.org/10.1016/j.actaastro.2017.09.003.

[13] Lavagna, M., Armellin, R., Bombelli, R., and Benvenuto, R., "Debris Removal Mechanism Based on Tethered Nets," *International Symposium on Artificial Intelligence, Robotics and Automation in Space*, 2012.

[14] Yue, S., Li, M., Zhao, Z., Du, Z., Wu, C., and Zhang, Q., "Parameter Analysis and Experiment Validation of Deployment Characteristics of a Rectangular Tether-Net," *Aerospace*, Vol. 10, No. 2, 2023. https://doi.org/10.3390/aerospace10020115, URL https://www.mdpi.com/2226-4310/10/2/115.

[15] Benvenuto, R., Salvi, S., and Lavagna, M., "Dynamics analysis and GNC design of flexible systems for space debris active removal," *Acta Astronautica*, Vol. 110, 2015, pp. 247–265. https://doi.org/https://doi.org/10.1016/j.actaastro.2015.01.014, URL https://www.sciencedirect.com/science/article/pii/S0094576515000296, dynamics and Control of Space Systems.

[16] Botta, E. M., Sharf, I., and Misra, A., "Evaluation of Net Capture of Space Debris in Multiple Mission Scenarios," *26th AAS/AIAA Space Flight Mechanics Meeting*, AAS, 2016, pp. 16–254.

[17] Shan, M., Guo, J., and Gill, E., "An analysis of the flexibility modeling of a net for space debris removal," *Advances in Space Research*, Vol. 65, No. 3, 2020, pp. 1083–1094. https://doi.org/https://doi.org/10.1016/j.asr.2019.10.041, URL https://www.sciencedirect.com/science/article/pii/S0273117719307914.

[18] Si, J., Pang, Z., Du, Z., and Cheng, C., "Dynamics Modeling and Simulation of Self-Collision of Tether-Net for Space Debris Removal," *Advances in Space Research*, Vol. 64, No. 9, 2019, pp. 1675–1687. https://doi.org/10.1016/j.asr.2019.08.006.

[19] Huang, W., Zou, H., Liu, H., Yang, W., Gao, J., and Liu, Z., "Contact dynamic analysis of tether-net system for space debris capture using incremental potential formulation," *Advances in Space Research*, Vol. 72, No. 6, 2023, pp. 2039–2050. https://doi.org/https://doi.org/10.1016/j.asr.2023.05.054, URL https://www.sciencedirect.com/science/article/pii/S0273117723004258.

[20] Hou, Y., Liu, C., Hu, H., Yang, W., and Shi, J., "Dynamic computation of a tether-net system capturing a space target via discrete elastic rods and an energy-conserving integrator," *Acta Astronautica*, Vol. 186, 2021, pp. 118–134. https://doi.org/https://doi.org/10.1016/j.actaastro.2021.05.029, URL https://www.sciencedirect.com/science/article/pii/S0094576521002666.

[21] Endo, Y., Kojima, H., and Trivailo, P. M., "Study on Acceptable Offsets of Ejected Nets from Debris Center for Successful Capture of Debris," *Advances in Space Research*, Vol. 66, No. 2, 2020, pp. 450–461. https://doi.org/10.1016/j.asr.2020.04.012.

[22] Endo, Y., Kojima, H., and Trivailo, P. M., "New Formulation for Evaluating Status of Space Debris Capture Using Tether-Net," *Advances in Space Research*, Vol. 70, No. 10, 2022, pp. 2976–3002. https://doi.org/10.1016/j.asr.2022.09.024.

[23] Chen, S., Woods, C. T., Boonrath, A., and Botta, E. M., "Analysis of the robustness and safety of net-based debris capture," *AIAA SCITECH 2022 Forum*, 2022, p. 1001.

[24] Forshaw, J. L., Aglietti, G. S., Fellowes, S., Salmon, T., Retat, I., Hall, A., Chabot, T., Pisseloup, A., Tye, D., Bernal, C., et al., "The Active Space Debris Removal Mission RemoveDebris. Part 1: From Concept to Launch," *Acta Astronautica*, Vol. 168, 2020, pp. 293–309. https://doi.org/10.1016/j.actaastro.2019.09.002.

[25] Aglietti, G. S., Taylor, B., Fellowes, S., Salmon, T., Retat, I., Hall, A., Chabot, T., Pisseloup, A., Cox, C., Mafficini, A., et al., "The Active Space Debris Removal Mission RemoveDebris. Part 2: In Orbit Operations," *Acta Astronautica*, Vol. 168, 2020, pp. 310–322. https://doi.org/10.1016/j.actaastro.2019.09.001.

[26] Ravichandra, N., and Botta, E. M., "Output Space Mapping for Net-Based Debris Capture," *AIAA Scitech 2020 Forum*, 2020. https://doi.org/10.2514/6.2020-0717.

[27] Barnes, C. M., and Botta, E. M., "A Quality Index for Net-Based Capture of Space Debris," *Acta Astronautica*, Vol. 176, 2020, pp. 455–463. https://doi.org/10.1016/j.actaastro.2020.06.044.

[28] Shah, R. K., Zeng, C., Botta, E. M., and Chowdhury, S., "Launch and Closure Optimization under Uncertainties for a Tether-Net Space Debris Capture System," *AIAA Aviation 2021 Forum*, 2021, p. 3103. https://doi.org/10.2514/6.2021-3103.

[29] Pelikan, M., Goldberg, D. E., Cantú-Paz, E., et al., "BOA: The Bayesian Optimization Algorithm," *Proceedings of the Genetic and Evolutionary Computation Conference*, Vol. 1, 1999, pp. 525–532.

[30] Snoek, J., Larochelle, H., and Adams, R. P., "Practical Bayesian Optimization of Machine Learning Algorithms," *Advances in Neural Information Processing Systems*, Vol. 25, edited by F. Pereira, C. Burges, L. Bottou, and K. Weinberger, Curran Associates, Inc., 2012. URL https://proceedings.neurips.cc/paper_files/paper/2012/file/05311655a15b75fab86956663e1819cd-Paper.pdf.

[31] Zeng, C., Hecht, G. R., Kumar, P. K., Shah, R. K., Botta, E. M., and Chowdhury, S., "Learning Robust Policies for Generalized Debris Capture with an Automated Tether-Net System," *AIAA SCITECH 2022 Forum*, 2022, p. 2379. https://doi.org/10.2514/6.2022-2379.

[32] Ghassemi, P., Mehmani, A., and Chowdhury, S., "Adaptive in Situ Model Refinement for Surrogate-Augmented Population-Based Optimization," *Structural and Multidisciplinary Optimization*, Vol. 62, 2020, pp. 2011–2034. https://doi.org/10.1007/s00158-020-02592-6.

[33] Brochu, E., Cora, V. M., and de Freitas, N., "A Tutorial on Bayesian Optimization of Expensive Cost Functions, with Application to Active User Modeling and Hierarchical Reinforcement Learning," , 2010. https://doi.org/https://doi.org/10.48550/arXiv.1012.2599.